analytical chemistry

Article

pubs.acs.org/ac

Aptamer/Graphene Quantum Dots Nanocomposite Capped Fluorescent Mesoporous Silica Nanoparticles for Intracellular Drug Delivery and Real-Time Monitoring of Drug Release

Fen-Fen Zheng, Peng-Hui Zhang, Yu Xi, Jing-Jia Chen, Ling-Ling Li,* and Jun-Jie Zhu*

State Key Laboratory of Analytical Chemistry and Collaborative Innovation Center of Chemistry for Life Sciences, School of Chemistry & Chemical Engineering, Nanjing University, Nanjing 210093, People's Republic of China

Supporting Information

ABSTRACT: Great challenges in investigating the release of drug in complex cellular microenvironments necessitate the development of stimuli-responsive drug delivery systems with real-time monitoring capability. In this work, a smart drug nanocarrier based on fluorescence resonance energy transfer (FRET) is fabricated by capping graphene quantum dots (GQDs, the acceptor) onto fluorescent mesoporous silica nanoparticles (FMSNs, the donor) via ATP aptamer for real-time monitoring of ATP-triggered drug release. Under extracellular conditions, the fluorescence of FMSNs remains in the "off" state in the low ATP level which is unable to trigger the release of drug. Once specifically recognized and internalized into the target tumor cells by AS1411 aptamer, in the ATP-rich cytoplasm, the conformation switch of the ATP aptamer causes the shedding of the GQDs from the nanocarriers, leading to the release of the loaded drugs and consequently severe cytotoxicity. Simultaneously, the fluorescence of FMSNs turns "on" along with the dissociation of GQDs, which allows real-time monitoring of the release of drug from the pores. Such a drug delivery system features high specificity of dual-target recognition with AS1411 and ATP aptamer as well as high sensitivity of the FRET-based monitoring strategy. Thus, the proposed multifunctional ATP triggered FRET-nanocarriers will find potential applications for versatile drug-release monitoring, efficient drug transport, and targeted cancer therapeutics.

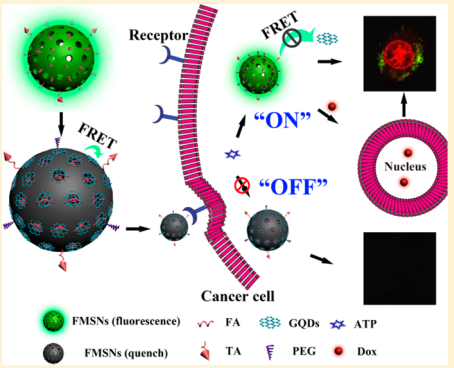

The concept of stimuli-responsive drug delivery was first suggested with the use of thermosensitive liposomes for the local release of drug through hyperthermia.[1] Since then, a lot of research has been carried out on stimuli-responsive systems for drug delivery.[2−8] An ideal stimuli-responsive drug delivery system should have the following characteristics: (i) recognize tumor microenvironment and target tumor cells in high selective manner, (ii) allow for tailored release profiles with spatial, temporal, and dosage control in response to exogenous or endogenous stimulus, (iii) monitor drug release in real time to ascertain actual drug concentrations at targeted area for avoiding insufficient or excess drug dosing.

To date, noninvasive and biocompatible mesoporous silica nanoparticles (MSNs) as efficient drug delivery carriers have attracted tremendous attention by virtue of their tunable pore size, unique porous structure, high specific surface area, good biocompatibility, and ease of surface functionalization.[9,10] Great progress in structural control and functional design has been achieved for bioapplications.[11,12] The ordered pore network of these MSNs can entrap drug within the pores. Importantly, the pores could be gated with various valves such as nanoparticles,[13−17] polymer multilayers,[18] DNA,[19,20] or proteins,[21] which were designed to trigger the release of the entrapped drug in the presence of external or internal stimuli including light,[22−24] temperature,[25−27] pH,[28−30] and biomolecules.[31−33] Although numerous stimuli-responsive MSNs for drug delivery have been reported, few has the capability of real-time monitoring, which remains a critical challenge.

Among all of the current real-time monitoring strategies, fluorescence imaging is one of the most sensitive techniques.[34] To follow the optical signal of the drug molecules themselves is the most ideal mode of monitoring drug release.[35,36] However, the majority of the drug candidates are neither fluorescent nor light-absorbent. Another possible way is to conjugate the drugs with caged dyes,[37,38] which may lead to drug structural change, thus affecting their therapeutic efficacy. Lee's group developed a novel FRET (fluorescence resonance energy transfer) based real-time monitoring system in drug delivery,[39] which consisted of coumarin-labeled-cysteine tethered mesoporous silica nanoparticles (MSNs) as the drug carrier, fluorescein isothiocyanate-β-cyclodextrin (FITC-β-CD) as the redox-responsive molecular valve to block the pores, and a FRET donor−acceptor pair of coumarin and FITC integrated within the pore-unlocking event. This provides a new strategy for real-time monitoring of drug release by using a nondrug based FRET donor−acceptor pair.

Received: August 4, 2015
Accepted: November 2, 2015

DOI: 10.1021/acs.analchem.5b03131
Anal. Chem. XXXX, XXX, XXX−XXX

Owing to its unique ability for DNA adsorption[40,41] as well as its super quenching capability, graphene is known to be a robust artificial nanomaterial in DNA analysis,[42,43] protein assays,[44] drug delivery,[45] etc. Graphene quantum dots (GQDs) maintain the intrinsic layered structural motif of graphene, but with smaller lateral size and abundant periphery carboxylic groups, and are more compatible with biological systems,[46,47] thus emerging as promising nanomaterials for DNA adsorbing and fluorescence quenching. Recently, Wang's group reported that GQDs had an attractive ability in drug delivery without any premodification due to their unique structural properties.[48] The GQDs could efficiently adsorb doxorubicin (Dox) molecules and quench their fluorescence. Therefore, the smaller size, excellent adsorption, and quenching capability of GQDs make them to be ideal capping motifs and FRET acceptors.

In this article, a multifunctional FRET-nanocarrier was fabricated by assembling the ATP aptamer (functionalization aptamer, FA) on the surface of fluorescent mesoporous silica nanoparticles (FMSNs) to form FA-FMSNs, which could strongly adsorb GQDs through $\pi-\pi$ stacking interaction and efficiently cap the pores of FMSNs as well as quench the fluorescence of FMSNs via FRET (Scheme 1). Moreover, ATP

Scheme 1. Preparation and Application of ATP-Responsive FRET Nanocarriers

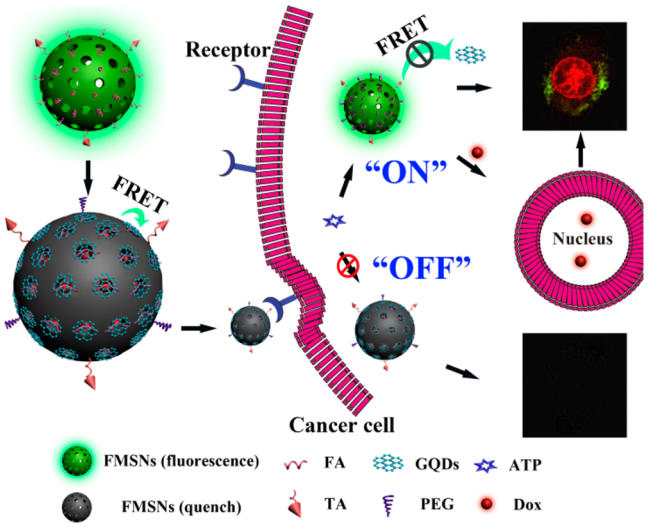

is present in low concentrations (<0.4 mM) in the extracellular environment but is relatively concentrated within the intracellular cytosol (1−10 mM).[49−52] This striking difference is beneficial in the design of ATP-mediated drug release systems.[53−55] Thus, once the FRET-nanocarriers were exclusively internalized into the target tumor cells by AS1411 aptamer (target aptamer, TA) recognition, the intracellular ATP served as a specific key to bind with ATP aptamer, inducing gradual desorption of GQDs from the mesopores and thereby triggering controlled drug release. The increase of fluorescence intensity due to the reduction of FRET from FMSNs to GQDs could be simultaneously used to monitor the drug release in real time.

EXPERIMENTAL SECTION

Preparation of FAG-FMSNs-TA-Dox-PEG (FRET-Nanocarriers). The synthesis of GQDs and amino-functionalized fluorescent mesoporous silica nanoparticles (FMSNs-NH_2) were described in the Supporting Information. The EDC/NHS method was used to conduct the conjugation of the aptamer molecules (ATP aptamer (FA) and AS1411 aptamer (TA), molar ratio1:5) and FMSNs-NH_2 to form FA-FMSNs-TA. The loading amounts of the aptamer strands on the FMSNs have been quantified by monitoring the fluorescence spectra of the aptamer (modified with FAM) in the supernatant (n_1) and in the stock solutions (n_2), the surface densities of the conjugated aptamer (d_3) on the FMSNs (m_3 = 1 mg) were calculated as follows: $d_3 = (n_2 - n_1)/m_3$, where the units of n, m, and d are nmol, mg, and nmol mg^{-1}, respectively. According to the amounts of the aptamer (10 nmol) added, the surface densities of the conjugated aptamer were 9.4 nmol mg^{-1}. First, Dox molecules were loaded into the FA-FMSNs-TA by incubating the nanoparticles (1.0 mg mL^{-1}) with different concentrations of Dox stock solutions in PBS (10 mM, 5 mM $MgCl_2$, 100 mM NaCl, pH 7.4) for 24 h. By centrifugation, the FA-FMSNs-TA-Dox and the supernatant were separated and collected. The Dox loading capacities were calculated by measuring the UV−vis spectra of the supernatant and stock solutions. Second, the sediment of FA-FMSNs-TA-Dox was dissolved in PBS (10 mM, 5 mM $MgCl_2$, 100 mM NaCl, pH 7.4), then different concentrations of GQDs were added and shaken at 37 °C. After 6 h, the FAG-FMSNs-TA-Dox were obtained by centrifugation and washing with PBS for three times. Through the interaction between FA and GQDs, the GQDs were capped onto the surfaces of the FA-FMSNs-TA-Dox to form FAG-FMSNs-TA-Dox. On the one hand, the GQDs could prevent the leakage of DOX from the mesopores. On the other hand, the GQDs also could quench the fluorescence of FMSNs by FRET from FMSNs to GQDs. Finally, FAG-FMSNs-TA-Dox-PEG was obtained by shaking the mixture of FAG-FMSNs-TA-Dox solution and mPEG-SPA stock solution (2 mg mL^{-1} in pH 7.4 PBS) at a speed of 200 rpm for 6 h. The mPEG-SPA, readily hydrolyzed in water to yield *N*-hydroxysuccinimide, was rapidly conjugated onto the nanoparticles by reacting with the amine residues originating from the APTES functionalization. The unreacted mPEG-SPA molecules were removed by two centrifugation/washing cycles.

Dox Release Experiments. The Dox loaded FRET-nanocarriers were incubated in 10 mM pH 7.4, 6.5, and 5.0 PBS for different amounts of time, respectively. After the addition of different concentrations of ATP stock solution, the Dox released from the FRET-nanocarriers was collected by centrifugation at 9300 rpm. The amount of released Dox in the supernatant solutions was measured by UV−vis spectrophotometry.

Cell Culture and Drug Release Monitoring. Human cervical carcinoma cells (HeLa cells) were obtained from Nanjing KeyGen Biotech Co. Ltd. and cultured in Dulbecco's Modified Eagle Medium (DMEM) at 37 °C under 5% CO_2 atmosphere, supplemented with L-glutamine (2 mM), penicillin (100 units mL^{-1}), streptomycin (100 μg mL^{-1}), and 10% fetal bovine serum (FBS). At the logarithmic growth phase, the cells were incubated with different nanoparticles in cultured medium for different times, then washed with PBS three times and cultured with fresh medium. The amounts of the FRET-nanocarriers internalized into the cells were evaluated by flow cytometry, while the drug release inside HeLa cells was monitored by CLSM. Cell viability was measured by MTT assay. Briefly, HeLa cells were cultured in a 96-well plate at a density of 10 000 cells in each well. After incubation for 24 h, the medium was replaced with 100 μL of fresh medium

DOI: 10.1021/acs.analchem.5b03131
Anal. Chem. XXXX, XXX, XXX−XXX

containing different concentrations of the nanoparticles. At the indicated time points (24 or 48 h), the medium was removed, and fresh medium (100 μL) containing MTT (10 μL, 5 mg mL^{-1}) was added into each well. After incubation for 4 h, the absorbance of the solution was measured to assess the relative viability of the cells using a ThermoFisher Scientific Varioskan Flash multifunctional microplate reader. The optical density (OD) was read at a wavelength of 492 nm. Relative cell viability was expressed as $([OD]_{test}/[OD]_{control}) \times 100\%$. Each experiment was repeated at least three times.

RESULTS AND DISCUSSION

Interaction between FA and GQDs. GQDs was synthesized according to our previously reported method.[56] The high-resolution transmission electron microscopy (HRTEM) shows that the GQDs have the average diameter of 4.5 nm (Figure S1a). The topographic heights of GQDs are mostly located between 0.5 and 1.5 nm with an average height of 1 nm, suggesting that most of GQDs are single layered or bilayered (Figure S1b). The cytotoxicity of the GQDs was measured by *in vitro* MTT (3-(4,5-dimethylthiazol-2-yl)-2,5-diphenyltetrazo-lium bromide) assay (Figure S1c). The cell viability of HeLa cells remained above 80% when they were treated by GQDs with a concentration up to 800 μg mL^{-1} for 48 h, indicating that GQDs have excellent biocompatibility.

To investigate the feasibility of the FA/GQD nanocomplexes as a stimuli-responsive gate, ATP-responsive experiment was carried out *in vitro* first. Briefly, ATP aptamer labeled with FAM (carboxy fluorescein) was incubated with GQDs to form FAM-FA/GQD nanocomplexes. The quenching ability of GQDs was estimated by measuring the fluorescence intensity of FAM-FA solution (100 nM) with different amounts of GQDs, ranging from 1 to 100 μg mL^{-1} (Figure 1b). Owing to the FRET process between FAM and GQDs, a gradual decrease of fluorescence intensity was observed with increasing amounts of GQDs assembled on the complex. Here, 100 μg mL^{-1} of GQDs was chosen as the optimized concentration with a quenching efficiency of 70%. In the presence of ATP, ATP aptamer could target ATP to form a hairpin configuration, thus dissociating ATP aptamer from the surface of GQDs and invalidating the FRET process. Consequently, obvious fluorescence recovery was observed by injecting ATP solution into the reaction system (Figure 1c).

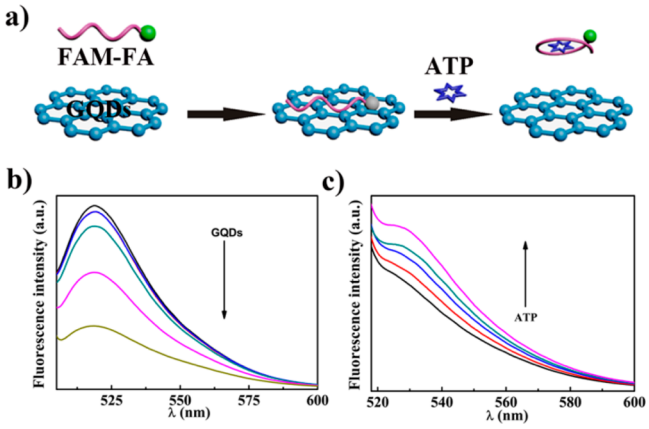

Figure 1. (a) Scheme of the interaction between ATP aptamer and GQDs. (b) Fluorescence emission spectra of 100 nM FAM-FA quenched by addition of GQDs with concentrations ranging from 10 to 100 μg mL^{-1}. (c) Fluorescence recovery of 10 nM FAM-FA/GQD nanocomplexes by addition of ATP (0, 0.05, 0.2, 0.8, 2 mM).

Fabrication and Characterization of FRET-Nanocarrriers. The FMSNs were synthesized by doping fluorescein isothiocyanate (FITC) into the mesoporous silica nanoparticles following the reported protocol with some modification.[57] The obtained FMSNs had a uniform size of 40 nm and displayed strong fluorescence and remarkable photostability, thus facilitating the tracking of the intracellular drug delivery and the real-time monitoring of drug release (Figure S2). These FMSNs were then functionalized with APTES and tethered with FA and TA via an amide bond. The average diameter of the GQDs was 4.5 nm, which could be preferable to cap the 2.7 nm-wide-pore. The Dox was selected as a model cargo, which was loaded into the pores of FMSNs by mixing FA-FMSNs-TA and Dox overnight (FA-FMSNs-TA-Dox). The Dox molecules with positive charge could diffuse into the pores of FMSNs and were trapped by the silanol residuals through hydrogen bonds and electrostatic interactions.[58,59] Then, the pores were capped with GQDs through π−π stacking interaction between FA and GQDs (FAG-FMSNs-TA-Dox), and the mPEG-SPA (SPA = succinyl propionate) was further conjugated to the FMSNs via the reaction between amine residues and SPA. Finally, the FRET-nanocarrriers (FAG-FMSNs-TA-Dox-PEG) was isolated by centrifugation after repeated washing. The fluorescence of the entrapped Dox could also be quenched by GQDs which could be used to verify the real-time monitoring efficiency of the FRET-nanocarriers. The amount of Dox loaded into FMSNs was determined to be 168 mg g^{-1} (Figure S8). And the drug amount remains nearly the same after it is treated with GQDs and PEG (Figure S9). The FRET-nanocarriers were well-dispersed in aqueous solutions due to the conjugation of hydrophilic PEG moieties on their surface.

Next, the assembly process of the FRET-nanocarrriers was characterized by TEM. Figure 2a shows that FMSNs and FA-FMSNs-TA has similar size with a mean diameter of 40 nm, while the size of FAG-FMSNs-TA-Dox-PEG has increased to 50 nm. Besides, the dynamic light scattering (DLS) result reveals that the hydrodynamic diameters of FMSNs, FA-FMSNs-TA, and FAG-FMSNs-TA are 58 nm, 72.5 nm, and 79 nm, respectively (Figure S3). The gradual increasing of the hydrodynamic diameter indicates the successful conjugation of FA and GQDs. The wormlike mesoporous structures with pore sizes of 2−3 nm and relatively high specific surface areas (373.427 m^2 g^{-1}) could be observed from the absence of corresponding small-angle X-ray diffraction peak(s) (Figure S4) and nitrogen adsorption−desorption isotherm measurements (Figure S5). Furthermore, the successful surface functionalization was confirmed by Fourier transform-infrared (FT-IR) spectroscopy and zeta potential measurement (Figures S6 and S7). As expected, the fluorescence of FMSNs-FA could be quenched by GQDs based on FRET similar to FAM-FA (Figure 2c). The loading amounts of the GQDs on the FA-FMSNs have been optimized to be 149 μg mg^{-1} by monitoring the fluorescence spectra of the GQDs in the supernatant and in the stock solutions (Figure S10). In addition, the remarkable fluorescence recovery of FMSNs further demonstrated that these FRET-nanocarriers could be used to monitor ATP-triggered drug release in real time (Figure 2d).

ATP-Responsive Controlled Drug Release and Correlating Drug Release to the FRET Signal *in Vitro*. Furthermore, to investigate the ATP-triggered uncapping efficiency of the FRET-nanocarrriers, drug release experiments

DOI: 10.1021/acs.analchem.5b03131
Anal. Chem. XXXX, XXX, XXX−XXX

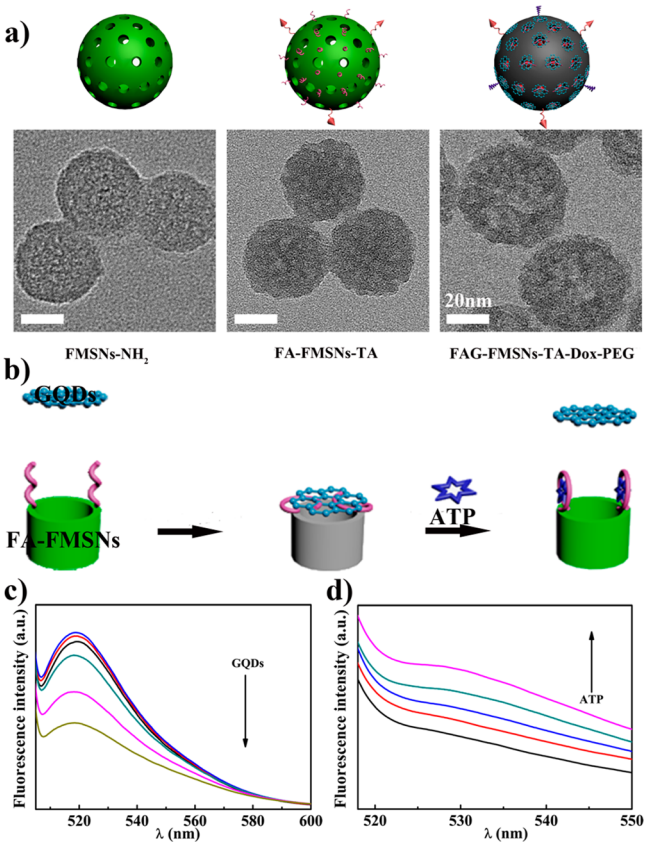

Figure 2. (a) Schemes (top) and TEM images (bottom) of FMSNs, FA-FMSNs-TA, and FAG-FMSNs-TA-Dox-PEG. (b) Scheme of the interaction between FA-FMSNs-TA and GQDs. (c) Fluorescence emission spectra of 1 mg mL^{-1} FA-FMSNs quenched by addition of GQDs with increased concentration (0, 10, 20, 50, 100, 200 μg mL^{-1}, respectively). (d) Fluorescence recovery of 1 mg mL^{-1} FAG-FMSNs by addition of ATP (0, 1, 2, 5, 10 mM, respectively).

were carried out at different levels of ATP. Real-time drug release profiles of the samples were recorded using a UV−vis spectrophotometer under the wavelength of 480 nm (Figure 3a, 1−4). In the absence of ATP, about 20% release of Dox was observed over a period of 48 h, indicating that the FRET-nanocarriers almost remained intact. While in the presence of different ATP amounts, an increase in the released Dox could

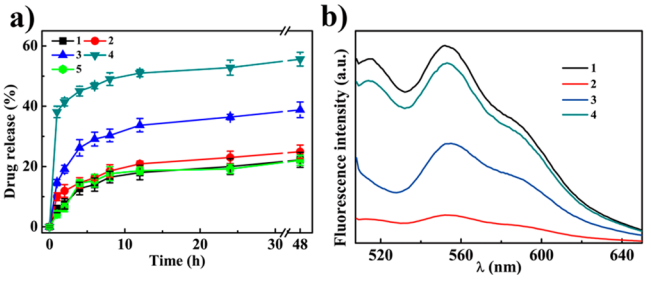

Figure 3. (a) (1−4) Release profiles of the FRET-nanocarrriers with addition of different concentrations of ATP in phosphate-buffered saline (PBS, 10 mM, pH = 5.0), the addition amounts of ATP were 0, 1, 5, 10 mM, respectively. (5) Release profiles of the G-FMSNs-Dox-PEG with addition of 10 mM of ATP in phosphate-buffered saline. (b) Fluorescence emission spectra of 0.1 mg mL^{-1} FA-FMSNs-TA-Dox (1) quenched with 200 μg mL^{-1} GQDs (2) and fluorescence recovery by adding of 5 mM ATP (incubated for 2 h (3) or for 4 h (4)).

be observed as time progressed. The percentage of Dox released from the FRET-nanocarriers was dependent on ATP concentrations, wherein concentrations of 5 mM or higher led to significantly faster and greater release of Dox. The release of Dox could reach a plateau within 4 h due to the rapid interaction between high concentrations of ATP and ATP aptamer. As a comparison test, G-FMSNs-Dox-PEG was prepared by the electrostatic interactions between GQDs and NH_2−FMSNs. Figure 3a, 5 shows that Dox entrapped in G-FMSNs-Dox-PEG cannot be released effectively even in high concentrations of triggers, which indicates that the dissociation of GQDs from the FRET-nanocarrers is due to the specific recognition and binding between ATP and FA. Considering the acidic extracellular microenvironment of tumor tissue, the stability of the drug delivery system was evaluated by determining the drug release in different buffers. As shown in Figure S11, the FA/GQD (FAG) valve could effectively prevent the release of Dox from the FRET-nanocarriers even in acidic environments (pH = 5). With the addition of ATP, rapid drug release was observed at the given pH values. It is worth noting that upon the addition of ATP, the drug release rate was independent of the pH changes. Additionally, selectivity studies toward ATP have been presented by probing the effects of different thymidine triphosphate analogues, TTP, CTP, GTP, on the unlocking process. The changes in fluorescence spectra of the Dox released from the nanocarriers treated by ATP, TTP, CTP, and GTP are described in Figure S12. Compared to the analogues, only ATP stimulates the effective release of Dox with a sharp increase of fluorescence intensity, indicating that the highly selective release of the nanocarriers was attributed to the specific recognition between ATP and FA.

In addition to behaving as three-dimensional gatekeepers to completely encapsulate the drugs in the nanocarriers, the aptamer/GQD nanocomplexes were proven to be electron acceptors for efficiently quenching the fluorescence of the FMSNs based on FRET (see above). This FRET property of the FRET-nanocarriers could be used to monitor the drug release from the pores. Because the modulation of FRET is integrated within the uncapping event, the corresponding change in the FRET signal can be used for monitoring the drug release at a temporal level. Meanwhile, since the release of Dox is rapid enough and only occurs when the pores are uncapped as a consequence of GQDs dissociation from the FRET-nanocarriers, there was probably a positive correlation between the drug release and the fluorescence recovery of FMSNs. As shown in Figure 3b, the addition of ATP to Dox-loaded FRET-nanocarriers induced the Dox release that was indicated by the fluorescence recovery of Dox. Simultaneously, a decrease in the FRET signal and thus the fluorescence turn-on of FMSNs was synchronized to the release of Dox. On the basis of this result, a positive correlation between the released Dox and FRET signal was obtained, which strongly indicated that the drug release could be monitored in real-time by the FRET signal change of the FRET-nanocarriers.

Specific Targeting and Traceability. Targeted delivery to cancer cells is essential in chemotherapy. Herein, the AS1411 aptamer, currently an anticancer agent under phase II clinical trials and also an aptamer to specifically recognize nucleolin overexpressed on the surfaces of some cancer cells,[60] was tethered to the FRET-nanocarriers as the target aptamer. The target efficiency and specificity of the FRET-nanocarriers were assessed by confocal laser scanning microscopy (CLSM) and

DOI: 10.1021/acs.analchem.5b03131
Anal. Chem. XXXX, XXX, XXX−XXX

flow cytometry analysis by determining the fluorescence of the loaded Dox (Figure S13). The fluorescence emission of released Dox for HeLa cells was higher than that for NIH 3T3 cells, which reflected the enhanced nanocarriers uptake due to the specific interaction between AS1411 aptamer and nucleolin. To further alleviate the side effects during cancer therapy, the FRET-nanocarriers was PEGylated, which could significantly minimize its nonspecific adsorption onto the NIH 3T3 cells.

CLSM was used to investigate the traceability of the FRET-nanocarriers during intracellular delivery and drug release. HeLa cells were cultured and incubated in cultured medium containing 20 μg mL^{-1} of the FRET-nanocarriers at 37 °C for a period of time. The cellular uptake and intracellular trafficking were investigated by monitoring the recovered fluorescence of FMSNs and Dox. After 2 h of incubation, FMSNs (green) and Dox (red) fluorescence signals were observed in HeLa cells. The FMSNs were mostly distributed in the cytoplasm, and the Dox was confirmed mostly in the cell nucleus by costaining with DAPI molecules (Figure S14). Lysosome staining experiment showed that most of the FRET-nanocarriers were trapped inside the endosome/lysosome, while some of them had successfully escaped into the cytoplasm (Figure S15). The high cytosolic ATP level led to a significant release of Dox, which specifically accumulated into the nuclei, intercalated into the twin-screw structure of DNA, inhibited macromolecular biosynthesis, and eventually induced cells death.

Intracellular ATP-Triggered Drug Release and Monitoring in Real-Time. We further investigated whether the FRET-nanocarriers could be used to monitor intracellular ATP-triggered drug release by detecting the fluorescence recovery of FMSNs and Dox. The HeLa cells were incubated with the FRET-nanocarriers for a different length of time. As expected, a time-course enhancement of Dox fluorescence in the cancer cells clearly indicated the controlled release of drugs from the FRET-nanocarriers. In the meantime, the gradual fluorescence recovery of FMSNs induced by DOX release was clearly detectable (Figure S16). This proves that the FRET-nanocarriers can respond to the presence of exogenous ATP by releasing the entrapped drug with concurrent change in the FRET signal. To demonstrate the intracellular ATP concentration-dependent Dox release from FRET-nanocarriers, we inhibited the ATP production in the cells by physically lowering the temperature (4 °C) and adding a chemical inhibitor, iodoacetic acid (IAA), prior to the addition of the FRET-nanocarriers. Cell incubation at 4 °C and adding IAA at 37 °C both led to a significant decrease in ATP generation within the cells (Figure 4a). The fluctuation in intracellular ATP concentration can result in a change in the extent of GQDs dissociation from the FRET-nanocarriers, which shall determine the FRET signal as well as the amount of Dox released. Correspondingly, flow cytometric results demonstrated the decrease of FMSNs fluorescence signal, which could be attributed to the down-regulation of ATP contents and reduced Dox release (Figure 4b). CLSM revealed that Dox release from FRET-nanocarriers was remarkable reduced in the cells that were incubated at 4 °C or treated with IAA at 37 °C, further confirming the monitoring capability of the FRET-nanocarriers for intracellular ATP-mediated drug release (Figure 4c).

Selective Toxicity. MTT tests were conducted to assess the tumoricidal potential of the established FRET-nanocarriers. HeLa cells and NIH-3T3 cells were incubated with different FRET-nanocarriers, respectively, in culture medium at 37 °C

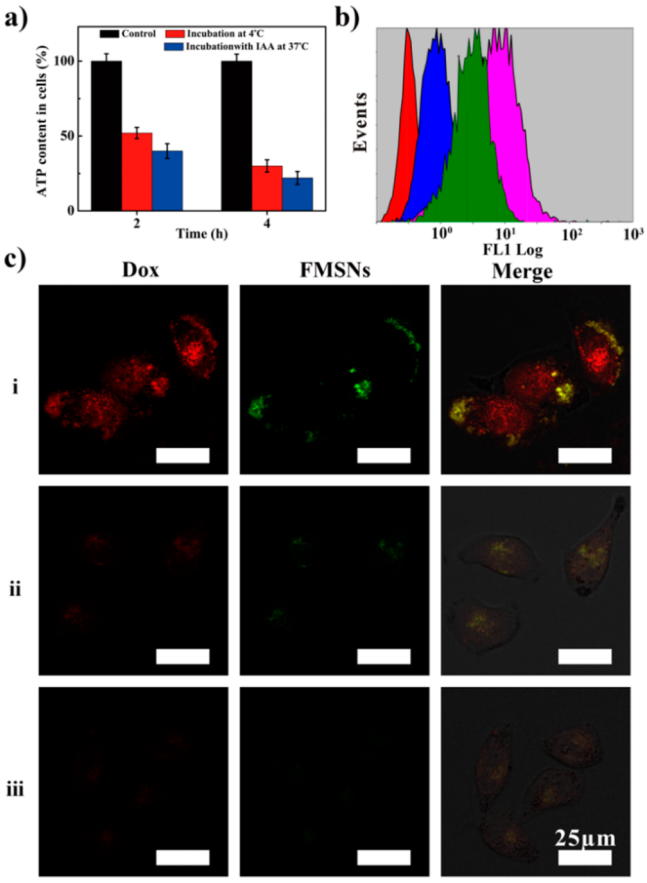

Figure 4. (a) ATP content in HeLa cells after different treatments; (b) fluorescence recovery of FMSNs obtained by flow cytometry (lines from left to right, control; incubation at 4 °C; incubation with IAA at 37 °C; incubation at 37 °C); (c) Dox released in HeLa cells of FAG-FMSNs-TA-Dox-PEG obtained using the CLSM. The cells were incubated with FAG-FMSNs-TA-Dox-PEG at 37 °C for 1 h and then incubated with the fresh culture medium at 37 °C for additional 2 h (i), incubated with IAA at 37 °C for additional 2 h (ii), or incubated at 4 °C for additional 2 h (iii) after removal of the excess FRET-nanocarriers.

for 24 or 48 h. As shown in Figure S17a, blank FRET-nanocarriers without Dox did not show cytotoxicity within the tested concentration range. Meanwhile, the efficient intracellular release of Dox from FAG-FMSNs-TA-Dox-PEG triggered by ATP provided higher cytotoxicity as compared to G-FMSNs-Dox-PEG which could not be uncapped by ATP. Specific lethality of the FRET-nanocarriers was investigated by incubating target cells (HeLa) with Dox, Dox-loaded FA-FMSNs and Dox-loaded FA-FMSNs-TA (Figure S17b). The lethality of free Dox at the microgram level was very small due to the drug efflux pump effect by ATP-binding cassette transporters from cytoplasm.[61] On the other hand, thanks to the AS1411 aptamer, the cellular uptake of FA-FMSNs-TA was higher than FA-FMSNs, which led to better anticancer activity. The MTT results shown in Figure 5 demonstrated that the toxicity of the FRET-nanocarriers without AS1411 aptamer and PEG modification was approximately equal toward NIH-3T3 cells and HeLa cells. After AS1411 aptamer and PEG modification, the FRET-nanocarriers exhibited much higher toxicity to HeLa cells than to NIH-3T3 cells due to the specific recognition of AS1411 aptamer and the antinonspecific adsorption by PEG. CLSM results have displayed the

DOI: 10.1021/acs.analchem.5b03131
Anal. Chem. XXXX, XXX, XXX−XXX

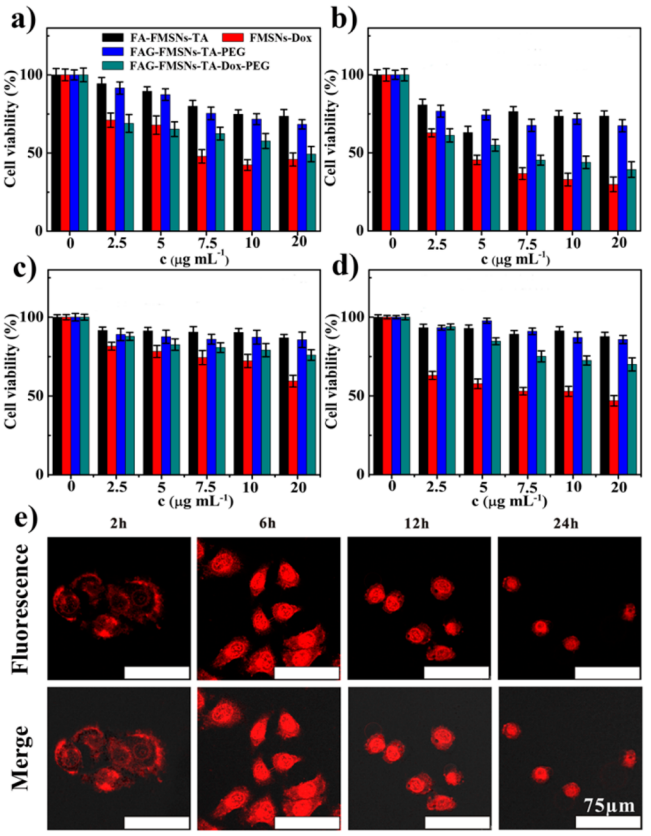

Figure 5. Cell viability of HeLa cells (a, b) and NIH 3T3 cells (c, d) incubated with different concentrations of FA-FMSNs-TA, FMSNs-Dox, FAG-FMSNs-TA-PEG, and FAG-FMSNs-TA-Dox-PEG for 24 and 48 h, respectively; (e) CLSM images of HeLa cells incubated with FAG-FMSNs-TA-Dox-PEG for different time durations.

therapeutic efficacy of the FRET-nanocarriers more visually (Figure 5e). A burst release of Dox was observed after the first 6 h owing to the uncapping by ATP. A mass of apoptotic bodies appeared after 24 h, which indicated that most of the cells were induced to apoptosis, suggesting a high therapeutic efficacy of the FRET-nanocarriers.

CONCLUSIONS

In summary, we have fabricated an ATP-responsive FRET-nanocarrier for intracellular drug delivery and real-time monitoring of drug release, wherein fluorescent mesoporous silica nanoparticles acted as scaffolds and aptamer−GQD nanocomplexes as capping and quenching motifs. It has been demonstrated that any exogenous or endogenous fluctuation in the ATP concentration can result in a change in drug release as well as concurrent variation in the FRET signal. The FRET-nanocarriers possess various attractive features. First, with the dual-target of AS1411 and ATP aptamer, the FRET-nanocarriers could release the drug more selectively in the cytoplasm of cancer cells. Second, the aptamer−GQD nanocomplexes behave as three-dimensional gatekeepers to completely encapsulate the drugs in the nanocarriers as well as electron acceptors to efficiently quench the fluorescence of the FMSNs. Third, the drug release was directly reflected by the recovery of the FMSNs along with the dissociation of the GQDs, which can be extended to any cargo without relying on the optical properties or the structural modification of the drugs. It is hoped this strategy could monitor intracellular drug concentrations and benefit successful chemotherapy for cancers.

ASSOCIATED CONTENT

Supporting Information

The Supporting Information is available free of charge on the ACS Publications website at DOI: 10.1021/acs.analchem.5b03131.

Additional experimental details and data (PDF)

AUTHOR INFORMATION

Corresponding Authors

*E-mail: lll-100@163.com.
*E-mail: jjzhu@nju.edu.cn.

Notes

The authors declare no competing financial interest.

ACKNOWLEDGMENTS

We gratefully appreciate the support from the National Basic Research Program (Grant 2011CB933502) of China and the National Natural Science Foundation (Grant Nos. 21335004, 21427807, and 21405078).

REFERENCES

(1) Yatvin, M. B.; Weinstein, J. N.; Dennis, W. H.; Blumenthal, R. *Science* **1978**, *202*, 1290−1293.
(2) Fleige, E.; Quadir, M. A.; Haag, R. *Adv. Drug Delivery Rev.* **2012**, *64*, 866−884.
(3) Ganta, S.; Devalapally, H.; Shahiwala, A.; Amiji, M. *J. Controlled Release* **2008**, *126*, 187−204.
(4) Mura, S.; Nicolas, J.; Couvreur, P. *Nat. Mater.* **2013**, *12*, 991−1003.
(5) Rapoport, N. *Prog. Polym. Sci.* **2007**, *32*, 962−990.
(6) Lu, Y.; Sun, W.; Gu, Z. *J. Controlled Release* **2014**, *194*, 1−19.
(7) Peterson, G. I.; Larsen, M. B.; Boydston, A. J. *Macromolecules* **2012**, *45*, 7317−7328.
(8) Zhang, P. H.; He, Z. M.; Wang, C.; Chen, J. N.; Zhao, J. J.; Zhu, X. N.; Li, C. Z.; Min, Q. H.; Zhu, J. J. *ACS Nano* **2015**, *9*, 789−798.
(9) Li, Z.; Barnes, J. C.; Bosoy, A.; Stoddart, J. F.; Zink, J. I. *Chem. Soc. Rev.* **2012**, *41*, 2590−2605.
(10) Zhang, X. Y.; Zhang, X. Q.; Wang, S. Q.; Liu, M. Y.; Zhang, Y.; Tao, L.; Wei, Y. *ACS Appl. Mater. Interfaces* **2013**, *5*, 1943−1947.
(11) Chen, Y.; Chen, H.; Zeng, D.; Tian, Y.; Chen, F.; Feng, J.; Shi, J. *ACS Nano* **2010**, *4*, 6001−6013.
(12) Zhang, P. H.; Cheng, F. F.; Zhou, R.; Cao, J. T.; Li, J. J.; Burda, C.; Min, Q. H.; Zhu, J. J. *Angew. Chem., Int. Ed.* **2014**, *53*, 2371−2375.
(13) Lai, C. Y.; Trewyn, B. G.; Jeftinija, D. M.; Jeftinija, K.; Xu, S.; Jeftinija, S.; Lin, V. S. Y. *J. Am. Chem. Soc.* **2003**, *125*, 4451−4459.
(14) Chen, P. J.; Hu, S. H.; Hsiao, C. S.; Chen, Y. Y.; Liu, D. M.; Chen, S. Y. *J. Mater. Chem.* **2011**, *21*, 2535−2543.
(15) Vivero-Escoto, J. L.; Slowing, I. I.; Wu, C. W.; Lin, V. S. Y. *J. Am. Chem. Soc.* **2009**, *131*, 3462−3463.
(16) Muhammad, F.; Guo, M.; Qi, W.; Sun, F.; Wang, A.; Guo, Y.; Zhu, G. *J. Am. Chem. Soc.* **2011**, *133*, 8778−8781.
(17) Chen, T.; Yu, H.; Yang, N. W.; Wang, M. D.; Ding, C. D.; Fu, J. J. *J. Mater. Chem. B* **2014**, *2*, 4979−4982.
(18) Zhu, Y.; Meng, W.; Gao, H.; Hanagata, N. *J. Phys. Chem. C* **2011**, *115*, 13630−13636.
(19) Climent, E.; Martinez-Manez, R.; Sancenon, F.; Marcos, M. D.; Soto, J.; Maquieira, A.; Amoros, P. *Angew. Chem.* **2010**, *122*, 7439−7441.
(20) Chen, C.; Geng, J.; Pu, F.; Yang, X. J.; Ren, J. S.; Qu, X. G. *Angew. Chem.* **2011**, *123*, 912−916.
(21) Wu, S.; Huang, X.; Du, X. *Angew. Chem.* **2013**, *125*, 5690−5694.
(22) Lu, J.; Choi, E.; Tamanoi, F.; Zink, J. I. *Small* **2008**, *4*, 421−426.

DOI: 10.1021/acs.analchem.5b03131
Anal. Chem. XXXX, XXX, XXX−XXX

(23) Ferris, D. P.; Zhao, Y. L.; Khashab, N. M.; Khatib, H. A.; Stoddart, J. F.; Zink, J. I. *J. Am. Chem. Soc.* **2009**, *131*, 1686−1688.
(24) Angelos, S.; Yang, Y. W.; Khashab, N. M.; Stoddart, J. F.; Zink, J. I. *J. Am. Chem. Soc.* **2009**, *131*, 11344−11346.
(25) Hong, C. Y.; Li, X.; Pan, C. Y. *J. Phys. Chem. C* **2008**, *112*, 15320−15324.
(26) Chung, P. W.; Kumar, R.; Pruski, M.; Lin, V. S. Y. *Adv. Funct. Mater.* **2008**, *18*, 1390−1398.
(27) Chang, B.; Sha, X.; Guo, J.; Jiao, Y.; Wang, C.; Yang, W. *J. Mater. Chem.* **2011**, *21*, 9239−9247.
(28) Casasus, R.; Climent, E.; Marcos, M. D.; Martinez-Manez, R.; Sancenon, F.; Soto, J.; Amoros, P.; Cano, J.; Ruiz, E. *J. Am. Chem. Soc.* **2008**, *130*, 1903−1917.
(29) Aznar, E.; Marcos, M. D.; Martınez-Manez, R.; Sancenon, F.; Soto, J.; Amoros, P.; Guillem, C. *J. Am. Chem. Soc.* **2009**, *131*, 6833−6843.
(30) Meng, H.; Xue, M.; Xia, T.; Zhao, Y. L.; Tamanoi, F.; Stoddart, J. F.; Zink, J. I.; Nel, A. E. *J. Am. Chem. Soc.* **2010**, *132*, 12690−12697.
(31) Kim, H.; Kim, S.; Park, C.; Lee, H.; Park, H. J.; Kim, C. *Adv. Mater.* **2010**, *22*, 4280−4283.
(32) Popat, A.; Ross, B. P.; Liu, J.; Jambhrunkar, S.; Kleitz, F.; Qiao, S. Z. *Angew. Chem.* **2012**, *124*, 12654−12657.
(33) Zhang, Z.; Balogh, D.; Wang, F.; Willner, I. *J. Am. Chem. Soc.* **2013**, *135*, 1934−1940.
(34) Chen, N. T.; Cheng, S. H.; Liu, C. P.; Souris, J. S.; Chen, C. T.; Mou, C. Y.; Lo, L. W. *Int. J. Mol. Sci.* **2012**, *13*, 16598−16623.
(35) Vivero-Escoto, J. L.; Slowing, I. I.; Trewyn, B. G.; Lin, V. S. Y. *Small* **2010**, *6*, 1952−1967.
(36) Fang, W. J.; Yang, J.; Gong, J. W.; Zheng, N. F. *Adv. Funct. Mater.* **2012**, *22*, 842−848.
(37) Weinstain, R.; Segal, E.; Satchi-Fainaro, R.; Shabat, D. *Chem. Commun.* **2010**, *46*, 553−555.
(38) Jana, A.; Devi, K. S. P.; Maiti, T. K.; Singh, N. D. P. *J. Am. Chem. Soc.* **2012**, *134*, 7656−7659.
(39) Lai, J.; Shah, B. P.; Garfunkel, E.; Lee, K. B. *ACS Nano* **2013**, *7*, 2741−2750.
(40) Lu, C. H.; Yang, H. H.; Zhu, C. L.; Chen, G. N. *Angew. Chem., Int. Ed.* **2009**, *48*, 4785−4787.
(41) Tang, Z. W.; Wu, H.; Cort, J. R.; Buchko, G. W.; Zhang, Y. Y.; Shao, Y. Y.; Aksay, I. A.; Liu, J.; Lin, Y. H. *Small* **2010**, *6*, 1205−1209.
(42) Postma, H. W. C. *Nano Lett.* **2010**, *10*, 420−425.
(43) Liu, X. Q.; Aizen, R.; Freeman, R.; Yehezkeli, O.; Willner, I. *ACS Nano* **2012**, *6*, 3553−3563.
(44) Chang, H. X.; Tang, L. H.; Wang, Y.; Jiang, J. H.; Li, J. H. *Anal. Chem.* **2010**, *82*, 2341−2346.
(45) Sun, X. M.; Liu, Z.; Welsher, K.; Robinson, J. T.; Goodwin, A.; Zaric, S.; Dai, H. J. *Nano Res.* **2008**, *1*, 203−212.
(46) Yan, X.; Li, B. S.; Li, L. S. *Acc. Chem. Res.* **2013**, *46*, 2254−2262.
(47) Li, L. L.; Wu, G. H.; Yang, G. H.; Peng, J.; Zhao, J. W.; Zhu, J. J. *Nanoscale* **2013**, *5*, 4015−4039.
(48) Wang, C.; Wu, C. Y.; Zhou, X. J.; Han, T.; Xin, X. Z.; Wu, J. Y.; Zhang, J. Y.; Guo, S. W. *Sci. Rep.* **2013**, *3*, 1−8.
(49) Traut, T. W. *Mol. Cell. Biochem.* **1994**, *140*, 1−22.
(50) Leist, M.; Single, B.; Castoldi, A. F.; Kuhnle, S.; Nicotera, P. *J. Exp. Med.* **1997**, *185*, 1481−1486.
(51) Gorman, M. W.; Feigl, E. O.; Buffington, C. W. *Clin. Chem.* **2006**, *53*, 318−325.
(52) Gribble, F. M.; Loussouarn, G.; Tucker, S. J.; Zhao, C.; Nichols, C. G.; Ashcroft, F. M. *J. Biol. Chem.* **2000**, *275*, 30046−30049.
(53) Zhang, Z. X.; Balogh, D.; Wang, F.; Willner, I. *J. Am. Chem. Soc.* **2013**, *135*, 1934−1940.
(54) Zhang, Z. X.; Balogh, D.; Wang, F.; Sung, S. Y.; Nechushtai, R.; Willner, I. *ACS Nano* **2013**, *7*, 8455−8468.
(55) Liao, W. C.; Lu, C. H.; Hartmann, R.; Wang, F.; Sohn, Y. S.; Parak, W. J.; Willner, I. *ACS Nano* **2015**, *9*, 9078−9086.
(56) Li, L. L.; Ji, J.; Fei, R.; Wang, C. Z.; Lu, Q.; Zhang, J. R.; Jiang, L. P.; Zhu, J. J. *Adv. Funct. Mater.* **2012**, *22*, 2971−2979.
(57) Pan, L. M.; He, Q. J.; Liu, J. N.; Chen, Y.; Ma, M.; Zhang, L. L.; Shi, J. L. *J. Am. Chem. Soc.* **2012**, *134*, 5722−5725.
(58) Doane, T. L.; Burda, C. *Chem. Soc. Rev.* **2012**, *41*, 2885−2911.
(59) Liu, J.; Bu, W.; Pan, L.; Shi, J. L. *Angew. Chem., Int. Ed.* **2013**, *52*, 4375−4379.
(60) Li, J. J.; Zhong, X. Q.; Cheng, F. F.; Zhang, J. R.; Jiang, L. P.; Zhu, J. J. *Anal. Chem.* **2012**, *84*, 4140−4146.
(61) He, Q. J.; Shi, J. L. *Adv. Mater.* **2014**, *26*, 391−411.

DOI: 10.1021/acs.analchem.5b03131
Anal. Chem. XXXX, XXX, XXX−XXX